

- square surface roughness ( $R$ ) of Au surfaces and Ag overlayers as a function of scan size after DMG of  $\sim 250$  ML of Ag. After  $H_2$  flame annealing of the Au(111) surface,  $R$  over a  $5 \mu\text{m}$  by  $5 \mu\text{m}$  area was typically in the range of 0.275 to 0.340 nm. After DMG,  $R$  was determined for the Ag overlayer (for example, over a  $5 \mu\text{m}$  by  $5 \mu\text{m}$  area,  $R = 0.336$  nm) and the Au surface over the identical area (for example,  $R = 0.392$  nm) by electrochemically stripping the layer in situ. The larger  $R$  of the Au surfaces after stripping of the Ag layer is related to submonolayer roughness that developed from surface alloying [S. G. Corcoran, G. S. Chakarova, K. Sieradzki, *J. Electroanal. Chem.* **337**, 85 (1994)].
26. The deposition current used corresponds to a flux of  $3.1 \times 10^{13}$  atoms  $\text{cm}^{-2} \text{s}^{-1}$  ( $0.02 \text{ ML s}^{-1}$ ). J. D. Porter and T. O. Robinson [*J. Phys. Chem.* **97**, 6696 (1993)] reported a value of  $1.4 \times 10^{-6} \text{ cm}^{-2} \text{s}^{-1}$  for the diffusivity of Ag adatoms on Ag(111) in electrolytes. Calculating the value of  $(4a^2D/J)^{1/6}$ , we obtained 50 nm as an order of magnitude estimate of the critical island size for our growth conditions.
27. J. Camarero et al., *Phys. Rev. Lett.* **81**, 850 (1998).
28. M. Dietterle, T. M. Will, D. M. Kolb, *Surf. Sci.* **342**, 29 (1995).
29. L. C. Feldman, J. W. Mayer, S. T. Picraux, *Materials Analysis by Ion Channeling* (Academic Press, New York, 1982), pp. 44–46.
30. The yield was determined as the area ratio of the Ag peaks for random alignment and the channeling alignment.

31. The sensitivity of Auger electron spectroscopy and Rutherford backscattering spectrometry is of order 0.5 and 1 atomic %, respectively. See, for example, M. P. Seah and D. Briggs, in *Practical Surface Analysis*, D. Briggs and M. P. Seah, Eds. (Wiley, New York, ed. 2, 1990), vol. 1, chap. 1.
32. K. Sieradzki, S. R. Brankovic, N. Dimitrov, unpublished data.
33. We thank B. Wilkens and R. Culbertson for assistance with the Rutherford backscattering spectrometry measurements and gratefully acknowledge the support of this work by the NSF, Division of Materials Research (contract DMR-9510663).

27 October 1998; accepted 26 February 1999

## Strongly Photonic Macroporous Gallium Phosphide Networks

Frank J. P. Schuurmans,<sup>1\*</sup> Daniël Vanmaekelbergh,<sup>2</sup>  
Jao van de Lagemaat,<sup>2†</sup> Ad Lagendijk<sup>1</sup>

A photo-assisted electrochemical etching technique to fabricate macropores in single-crystalline gallium phosphide (GaP) with variable porosity has been developed. Scanning electron microscopy and x-ray diffraction experiments confirm that the material consists of three-dimensional, interconnected random networks with pore sizes of about 150 nanometers. Optical transmission measurements demonstrate that the nonabsorbing disordered structures strongly scatter light. The photonic strength is controlled by filling the pores with liquids of different refractive indices. Macroporous gallium phosphide filled with air has the highest scattering efficiency for visible light.

In a binary system with components of refractive indices  $n_1$  and  $n_2$ , the efficiency of light scattering depends on how these components are organized in the system, the dimensions of the components, and the refractive index ratio  $n_1/n_2 = m$ . Scattering of light is strongest if  $m$  is large and the length scale of refractive index variation,  $s$ , is comparable to the wavelength of light  $\lambda$ . This regime has received much attention in the search for strongly scattering (photonic) materials. For ordered systems with a periodic variation in the refractive index, that material is a photonic crystal. Such crystals feature photonic band gaps (1, 2): frequency ranges for which light will not propagate in the crystal because of multiple Bragg reflections. If the material is disordered, the interference of scattered light ultimately leads to Anderson localization (3, 4). Photonic band gaps and Anderson localization are closely related. Both inhibit light propagation due to interference (not absorption) and can only be obtained for strong-

ly photonic materials, those with  $m \sim 3$  or larger.

For infrared light, Anderson localization has been reported for gallium arsenide powders ( $m \approx 3.5$ ) (4), and a two-dimensional (2D) photonic band gap has been reported for macroporous Si ( $m \approx 3.4$ ) (5). In the visible, considerable progress has been made by the preparation of 3D air-sphere crystals of  $\text{TiO}_2$  ( $m \approx 2.7$ ) (2). Inhibition of the propagation of visible light has not yet been reported for 3D structures—apparently larger values of  $m$  ( $>2.7$ ) are needed. Obviously,  $m$  is a crucial parameter for photonic materials. In addition to large  $m$ , it is thus desirable to have the ability to tune  $m$ , allowing investigation of its importance for the photonic strength.

We report here on the optical scattering properties of electrochemically etched, macroporous, single-crystalline gallium phosphide (GaP). The 3D random network of GaP is completely interconnected, as observed by scanning electron microscopy (SEM) and confirmed by x-ray diffraction. An important consequence of the macroporous network is that we are able to modify the refractive index ratio by filling the voids with materials with different refractive indices without disturbing the overall porous structure. GaP has a large refractive index of  $\sim 3.3$  and an indirect band gap of 2.24 eV (550 nm) (6), which allows the preparation of strongly photonic systems ( $m \approx 3.3$ ) with negligible absorption in the red part of the

visible spectrum. Using an etching technique, we prepared slabs of strongly scattering, random GaP networks with structural units of about 150 nm and two different porosities, 35 and 50%. Furthermore, the method makes it possible to control the thickness of the scattering slab.

The macroporous GaP structure is formed by anodic etching of n-type GaP single crystals (donor density,  $2 \times 10^{17} \text{ cm}^{-3}$ ) under dielectric breakdown conditions (7–9). The 350- $\mu\text{m}$ -thick polished wafers are mounted with a (100) face exposed to the 0.5 M  $\text{H}_2\text{SO}_4$  electrolyte. Application of a strong positive potential (15 V versus normal hydrogen electrode) leads to severe band bending at the n-GaP/electrolyte interface. Interband tunneling of electrons (10) from the valence band or from band gap states to the conduction band takes place, generating holes at the surface, which are consumed in anodic dissolution of the GaP. The generation of holes is spatially nonuniform, which results in the porous network growing deeper into the GaP crystal. The anodic charge is proportional to the thickness of the porous structure  $L$ , enabling coulometric control of this important parameter (9). A SEM micrograph of a cross section of the porous slab is used to calibrate the linear charge-thickness relation. The porosity is determined to be  $\sim 35$  volume % of air. We prepared a series of samples with porous slab thicknesses ranging from 5 to 120  $\mu\text{m}$ .

In addition to the anodically etched GaP (A-GaP), we also prepared photoanodically etched GaP (PA-GaP) samples. Exploiting a technique that uses homogeneous photo-assisted etching, we are able to prepare slabs with a higher porosity. A-GaP samples are subjected to a further process of photoanodic etching in a  $\text{H}_2\text{O}:\text{H}_2\text{SO}_4:\text{H}_2\text{O}_2$  electrolyte solution, using 50 mW of 1.96-eV sub-band gap light from a HeNe laser. Photons are absorbed by a transition of an electron from the top of the valence band to an interfacial state, 0.3 eV below the conduction band, followed by thermal release of the interfacial electron into the conduction band (11). The remaining hole is involved in anodic dissolution. Because of the weak absorption of the light in the porous structure, the etch rate is

<sup>1</sup>Van der Waals-Zeeman Instituut, Universiteit van Amsterdam, Valckenierstraat 65, 1018 XE Amsterdam, The Netherlands. <sup>2</sup>Debye Instituut, Universiteit Utrecht, Post Office Box 80000, 3508 TA Utrecht, The Netherlands.

\*To whom correspondence should be addressed. E-mail: schuurma@phys.uva.nl

†Present address: Basic Sciences Center, National Renewable Energy Laboratory, 1617 Cole Boulevard, Golden, CO 80401-3393, USA.

## REPORTS

constant across the porous network and the porosity of the sample is increased uniformly, controlled by the photoanodic etch charge. In such a way, we prepared PA-GaP with slab thicknesses between 5 and 60  $\mu\text{m}$  and an increased estimated porosity of about 50%. Further etching results in mechanically unstable samples, probably because the rigidity percolation threshold is reached (12).

A SEM micrograph of the porous structure of PA-GaP (Fig. 1) reveals that the structure is random. A detailed and quantitative analysis of the PA-GaP structure is obtained from the autocorrelation function [also known as the Patterson function (13)], which represents the spatial correlation of the GaP structures or, equivalently, the air structure in between. The autocorrelate is not circular symmetric but slightly elongated, indicating a preferential direction. PA-GaP is characterized by two correlation lengths, along and perpendicular to this direction, for which we find  $155 \pm 8$  and  $108 \pm 6$  nm, respectively. Analysis of the SEM pictures from different parts of the porous sample show the same values for the two correlation lengths, which is a characteristic of a statistically homogeneous material. Furthermore, the slight asymmetry in the autocorrelate is connected to preferential etching along certain crystallographic axes (7), also indicated by the somewhat triangular shape of the GaP entities. However, for different parts of the porous structure, the direction was along different crystallographic axes, among which no correlation could be detected. Therefore, the entire sample on average is considered to be isotropic and homogeneous.

To the eye, bulk GaP is transparent and orange, whereas A-GaP is dark yellow and the PA-GaP samples are bright whitish yellow, in-

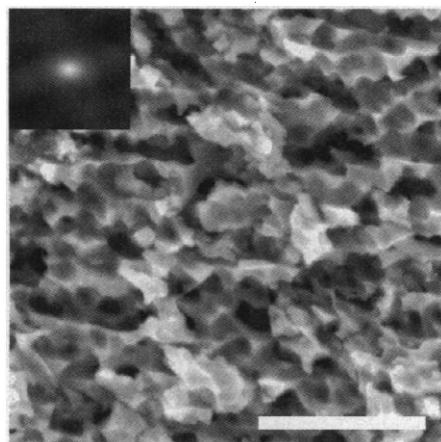


**Fig. 1.** SEM micrograph of PA-GaP and (inset) its autocorrelate. The lighter areas correspond to GaP and the dark parts to the pores. The typical size of the GaP entities is about 150 nm, as concluded from the autocorrelate. The porous structure is statistically homogeneous and isotropic. Scale bar, 1  $\mu\text{m}$ .

dicating that PA-GaP scatters light more strongly than A-GaP, as apparently for PA-GaP relatively more blue light is scattered out before it is absorbed. The scattering efficiency is measured quantitatively by determining the total light transmission through the porous slab as a function of its thickness  $L$ .

Total transmission measurements were done at 685 nm (1.81 eV) (14). The transmitted diffuse light intensity was collected with a 3-inch  $\text{BaSO}_4$  integrating sphere (Labsphere) and measured with a silicon diode detector. In order to obtain an absolute value of the total transmission, the measurements are normalized to incident light intensity, where we take into account the loss due to the specular reflection. In Fig. 2, the inverse total transmission versus the porous slab thickness  $L$  is shown. The measurements are described by classical diffusion with negligible absorption, as is evident from the linear dependence (15, 16). To quantitatively infer the scattering mean free path from these measurements, internal reflection corrections (17, 18) need to be incorporated in diffusion theory. As the effective refractive index  $n_e$  of our samples is not equal to 1, diffuse light will be reflected at the porous slab interfaces, modifying the transmission coefficient. For nonabsorbing media, the total transmission coefficient (19) is

$$T = \frac{1 + z_e}{(L/\ell) + 2z_e} \quad (1)$$

Here  $\ell$  is the transport mean free path (the average distance light propagates before its direction is randomized) and  $z_e$  is the extrapolation length ratio, which depends on the diffuse reflection coefficient (18, 19). Given the extrapolation length ratios (20) and using

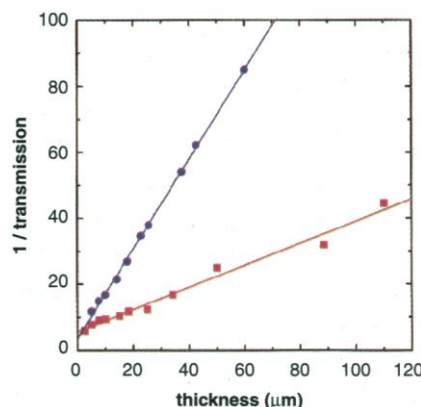


**Fig. 2.** The inverse total transmission as a function of the porous slab thickness, measured at 685 nm. The red squares correspond to A-GaP and the blue circles to PA-GaP. The solid lines are calculated with diffusion theory with negligible absorption, giving excellent agreement with the data. The transport mean free paths are inferred from the slope, resulting in  $0.47 \pm 0.05$   $\mu\text{m}$  and  $0.17 \pm 0.02$   $\mu\text{m}$  for A-GaP and PA-GaP, respectively.

Eq. 1, it is easy to extract the transport mean free paths from the measurements. For A-GaP,  $\ell = 0.47 \pm 0.05$   $\mu\text{m}$ , and for PA-GaP,  $\ell = 0.17 \pm 0.02$   $\mu\text{m}$ . To compare the scattering properties of our samples, we also calculate the values of  $k_e \ell = (2\pi/\lambda)n_e \ell$ , the standard measure of inverse scattering efficiency, giving  $k_e \ell = 8.6 \pm 0.5$  (A-GaP) and  $k_e \ell = 2.6 \pm 0.2$  (PA-GaP). The photoanodic etching treatment enhances this efficiency by more than a factor of 3, resulting in the most strongly scattering material for visible light reported to date (21).

From the single spots in the x-ray diffraction pattern, it is concluded that after etching, the porous layer is still single-crystalline GaP, meaning that the network is completely interconnected. As a result, the material is mechanically stable and can be filled with liquids. We measured diffuse light transmission through a 50- $\mu\text{m}$ -thick sample filled with nonabsorbing liquids of different refractive indices, ranging from 1.33 to 1.54 (Fig. 3). The transmission increases because of the decrease in the refractive index ratio  $m$  between the voids and GaP, with the largest increase (by a factor of 2.6) for the higher porosity material PA-GaP. For samples much thicker than the extrapolation length ( $L \gg z_e \ell$ ), it is seen from Eq. 1 that the relative increase of transmission matches the relative increase of  $\ell$ . Therefore, we directly measure the dependence of the scattering efficiency on refractive index ratio  $m$  of one microscopic

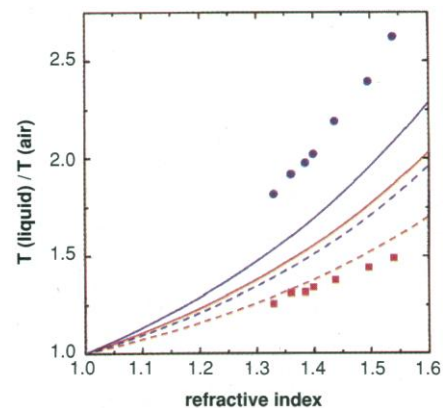


**Fig. 3.** Transmission of light through A-GaP (red squares) and PA-GaP (blue circles) filled with liquids, normalized to the transmission of the air-filled sample, as a function of the refractive index of the liquid. The increase in transmission matches the increase in  $\ell$ , which is a direct measure of the opacity. Results from effective medium theories are shown for comparison: Maxwell Garnett (dashed lines) theory and Bruggeman theory (solid lines). The models are plotted for the two corresponding volume fractions: 35% of air for A-GaP (red) and 50% for PA-GaP (blue). Although both models qualitatively describe the dependence of  $\ell$  on the porosity and refractive index ratio, no quantitative agreement could be obtained.

scattering realization. Also plotted in Fig. 3 for comparison are results from effective medium theories (22, 23), which depend only on the porosity and refractive index ratio. The morphology of the scattering material determines which effective medium model is applicable (22). Maxwell Garnett theory was developed for spherical scatterers in a homogeneous dielectric background (22), whereas Bruggeman's approach (16) treats both dielectric components on a symmetrical basis and seems to be the better choice for porous GaP. Both the porosity and the refractive index ratios of our samples are known. The two effective medium theories are compared with experimental results without any adjustable parameters. As can be seen, our measurements are not quantitatively described by existing effective medium models, which prompts the need to develop new theories. In fact, an effective medium approach is not expected to apply, because it was developed for weakly scattering media with  $s \ll \lambda$  and relatively small  $m$ . It is therefore not surprising that the discrepancy between theory and experiment is largest for the most strongly scattering material, PA-GaP. As observed, a relatively small decrease in refractive index ratio, from 3.26 to 2.12, leads to a large modification of the scattering efficiency, establishing the importance of the refractive index ratio for strongly photonic materials.

#### References and Notes

1. E. Yablonovitch, *Phys. Rev. Lett.* **58**, 2059 (1987); S. John, *ibid.*, p. 2486.
2. B. T. Holland, C. F. Blanford, A. Stein, *Science* **281**, 538 (1998); J. E. G. J. Wijnhoven and W. L. Vos, *ibid.*, p. 802.
3. P. W. Anderson, *Phys. Rev.* **109**, 1492 (1958); S. John, *Phys. Rev. Lett.* **53**, 2169 (1984); P. W. Anderson, *Philos. Mag. B* **52**, 505 (1985).
4. D. S. Wiersma, P. Bartolini, A. Lagendijk, R. Righini, *Nature* **390**, 671 (1997).
5. U. Grüning, V. Lehmann, S. Ottow, K. Busch, *Appl. Phys. Lett.* **68**, 747 (1996).
6. D. E. Aspnes and A. A. Studna, *Phys. Rev. B* **27**, 985 (1983).
7. B. D. Chase and D. B. Holt, *J. Electrochem. Soc.* **119**, 314 (1972).
8. B. H. Erné, D. Vanmaekelbergh, J. J. Kelly, *Adv. Mater.* **7**, 739 (1995).
9. F. Irazzo Marín, M. A. Hamstra, D. Vanmaekelbergh, *J. Electrochem. Soc.* **143**, 1137 (1996).
10. C. Zener, *Proc. R. Soc. London* **145**, 523 (1934).
11. D. Vanmaekelbergh and L. van Pieterse, *Phys. Rev. Lett.* **80**, 821 (1998).
12. W. Bresser, P. Boolchand, P. Suranyi, *ibid.* **56**, 2493 (1986).
13. B. E. Warren, *X-ray Diffraction* (Dover, New York, 1990).
14. From previous electrochemical experiments, it is known that the photoanodic etching current density at this wavelength was below the detection limit, indicating that the amount of light absorption is undetectably small.
15. A. Ishimaru, *Wave Propagation and Scattering in Random Media*, vols. I and II (Academic Press, New York, 1978); A. Z. Genack, *Phys. Rev. Lett.* **58**, 2043 (1987).
16. P. Sheng, *Introduction to Wave Scattering, Localization, and Mesoscopic Phenomena* (Academic Press, San Diego, CA, 1995).
17. A. Lagendijk, R. Vreeker, P. de Vries, *Phys. Lett. A* **136**, 81 (1989).
18. J. X. Zhu, D. J. Pine, D. A. Weitz, *Phys. Rev. A* **44**, 3948 (1991).
19. D. J. Durian, *Phys. Rev. E* **50**, 857 (1994).
20. For A-GaP,  $n_e$ , which depends on the porosity, is estimated to be  $2.0 \pm 0.1$ , corresponding to  $z_e = 5.4 \pm 0.6$ . Whereas for the higher porosity medium, PA-GaP,  $n_e = 1.7 \pm 0.1$  and thus  $z_e = 3.4 \pm 0.5$ .
21. D. S. Wiersma, M. P. van Albada, B. A. van Tiggele, A. Lagendijk, *Phys. Rev. Lett.* **74**, 4193 (1995).
22. R. Landauer, *Electrical Transport and Optical Properties of Inhomogeneous Media*, J. C. Garland and D. B. Tanner, Eds. [American Institute of Physics (AIP) Conference Proceedings No. 40, AIP, New York, 1978].
23. W. Lamb, D. M. Wood, N. W. Ashcroft, *Phys. Rev. B* **21**, 2248 (1980); S. Datta, C. T. Chan, K. M. Ho, C. M. Soukoulis, *ibid.* **48**, 14936 (1993); K. Busch and C. M. Soukoulis, *Phys. Rev. Lett.* **75**, 3442 (1995).
24. We thank J. Gómez Rivas for valuable discussions, P. de Jongh for taking the SEM pictures, and Philips Research Laboratories (Eindhoven, The Netherlands) for supplying the GaP crystals. This work is part of the research program of the Stichting voor Fundamenteel Onderzoek der Materie, which is financially supported by the Nederlandse Organisatie voor Wetenschappelijk Onderzoek.

24 December 1998; accepted 1 March 1999

## Multilineage Potential of Adult Human Mesenchymal Stem Cells

Mark F. Pittenger,<sup>1\*</sup> Alastair M. Mackay,<sup>1</sup> Stephen C. Beck,<sup>1</sup> Rama K. Jaiswal,<sup>1</sup> Robin Douglas,<sup>1</sup> Joseph D. Mosca,<sup>1</sup> Mark A. Moorman,<sup>1</sup> Donald W. Simonetti,<sup>1</sup> Stewart Craig,<sup>1</sup> Daniel R. Marshak<sup>1,2</sup>

Human mesenchymal stem cells are thought to be multipotent cells, which are present in adult marrow, that can replicate as undifferentiated cells and that have the potential to differentiate to lineages of mesenchymal tissues, including bone, cartilage, fat, tendon, muscle, and marrow stroma. Cells that have the characteristics of human mesenchymal stem cells were isolated from marrow aspirates of volunteer donors. These cells displayed a stable phenotype and remained as a monolayer in vitro. These adult stem cells could be induced to differentiate exclusively into the adipocytic, chondrocytic, or osteocytic lineages. Individual stem cells were identified that, when expanded to colonies, retained their multilineage potential.

Recently, pluripotent stem cells have been cultured from human fetal tissue and have shown the ability to give rise to a variety of differentiated cell types found in embryonic germ layers (1). Many adult tissues contain populations of stem cells that have the capacity for renewal after trauma, disease, or aging. The cells may be found within the tissue or in other tissues that serve as stem cell reservoirs. For example, although bone marrow is the major source of adult hematopoietic stem cells (HSCs) that renew circulating blood elements, these cells can be found in other tissues (2). The adult bone marrow also contains mesenchymal stem cells (MSCs), which contribute to the regeneration of mesenchymal tissues such as bone, cartilage, muscle, ligament, tendon, adipose, and stroma (3–5). In vitro and animal implant studies (5–10) have indicated that there is either a multipotent MSC or the populations are mixtures of committed progenitor cells, each with re-

stricted potential. We report the isolation, expansion, and characterization of the multipotent human MSC (hMSC).

We characterized an isolated population of homogeneous human mesenchymal cells from bone marrow taken from the iliac crest (5) (see Web Fig. 1, available at [www.sciencemag.org/feature/data/983855.sh1](http://www.sciencemag.org/feature/data/983855.sh1)). Previous studies have identified selection criteria for fetal bovine serum (FBS) that allows the expansion of a marrow cell population with MSC potential after implantation (5, 11). The mesenchymal cells described here were characterized by their ability to proliferate in culture with an attached well-spread morphology (Fig. 1, A and B), by the presence of a consistent set of marker proteins on their surface (Fig. 1, C and D) (12–14), and by their extensive consistent differentiation to multiple mesenchymal lineages under controlled in vitro conditions (Fig. 2).

A density gradient was used in the isolation procedure to eliminate unwanted cell types that were present in the marrow aspirate. A small percentage (estimated at about 0.001 to 0.01%) of cells isolated from the density interface of 1.073 g/ml attached and grew as fibroblastic cells that developed into

<sup>1</sup>Osiris Therapeutics, 2001 Aliceanna Street, Baltimore, MD 21231-3043, USA. <sup>2</sup>Johns Hopkins University, School of Medicine, Baltimore, MD 21205, USA.

\*To whom correspondence should be addressed. E-mail: mpittenger@osiristx.com